

## Supporting Information to

# Dual-channel RESOLFT nanoscopy by fluorescence kinetics

*Ilaria Testa, Elisa D'Este, Nicolai T. Urban, Francisco Balzarotti, Stefan W. Hell*

Department of NanoBiophotonics, Max Planck Institute for Biophysical Chemistry,  
Göttingen, Germany;

Correspondence to [shell@gwdg.de](mailto:shell@gwdg.de) (SWH); [itesta@gwdg.de](mailto:itesta@gwdg.de) (IT)

### **Organotypic hippocampal slice preparation.**

Hippocampal brain slices were prepared by dissecting hippocampi from postnatal day P5–P7 wildtype C57BL/6 mice, which were then sectioned in 400  $\mu\text{m}$  thick slices and embedded in a plasma clot on 0.14 mm thick glass coverslips. The slices were maintained in a roller incubator at 35°C in medium containing (in ml): BME 97, HBSS 50, horse serum 50, glucose (5M) 2, glutamine (200mM) 1 — according to the method of Gähwiler et al. 1997<sup>1</sup>. Slice cultures were left to mature for 12 days in the incubator and were used in the experiments up to an age of 45 days *in vitro* after preparation. For transfection we injected the viruses into the CA1- and CA3-regions of the slice cultures using a patch pipette connected to a pressure generator (Tooheyspritzer, Toohey Company, Fairfield, NJ, USA). The cultures were then incubated for at least 12 hours and imaged within 12–48 hours after transfection. For imaging, brain slices were transferred to an imaging chamber and maintained in artificial cerebrospinal fluid (ACSF) containing (in mM) NaCl 126, KCl 2.5, CaCl<sub>2</sub> 2.5, MgCl<sub>2</sub> 1.3, glucose 30 and HEPES 27; the pH was adjusted with NaOH to 7.4.

### **Primary hippocampal neuron culture preparation.**

Cultures of hippocampal neurons were prepared from Wistar rats of mixed sex at postnatal day P0–P1 in accordance with the regulations of the German Animal Welfare Act and under the approval of the local veterinary service. Cells were plated on 100  $\mu\text{g}/\text{ml}$  polyornithine (Sigma-Aldrich, cat. P3655) and 1  $\mu\text{g}/\text{ml}$  laminin (BD Bioscience, cat. 354232)-coated coverslips. Neuronal cultures were maintained in Neurobasal medium (Gibco, cat. 21103049)

supplemented with 2% B27 serum-free supplement (Gibco, cat. 17504044), 2 mM L-glutamine (Gibco, cat. 25030) and pen/strep (100 units/ml and 100 µg/ml, respectively, BiochromAG, cat. A2213). On the day after plating, 5 µM cytosine β-D-arabinofuranoside (Sigma, cat. C1768) was added to the cultures. Medium was replaced once per week. Cells were infected with viruses 12–48 hours prior to experiments. Imaging was performed in ACSF buffer.

## **Viruses**

Transfections were performed using modified Semliki Forest Viruses (SFV) carrying different pSCA3 sequences. The plasmids used to generate the SFVs were engineered from pSCA3-LifeAct-DronpaM159T<sup>2</sup> by replacing the rsFP or the targeting sequence. We generated pSCA3-LifeAct-rsEGFPN205S, pSCA3-rat-homer1c-DronpaM159T and pSCA3-rat-homer1c-rsEGFPN205S, pSCA3-Mito-DronpaM159T and pSCA3-Mito-rsEGFPN205S. The Mito sequence was derived from the Clontech pDsRed2-Mito vector.

## RESOLFT nanoscopy

RESOLFT nanoscopy overcomes the diffraction barrier by coordinate-targeted switching of fluorescent molecules using a light pattern featuring one or more intensity minima (zeros). In single-point scanning implementations, such as the one used here, the off-switching focal beam is ring-shaped with an intensity zero (minimum) at the center. Its role is to transiently silence the emission of fluorophores by switching them to metastable off-states. Reversible photoswitchable proteins (rsFPs) can be converted from a fluorescent (ON) into a non-fluorescent dark state (OFF) and vice versa by illumination with different wavelengths. Here we used 405nm for on- and 491nm for off-switching. Once switched off, the rsFPs cannot be excited anymore and remain dark. Only fluorophores residing in the direct vicinity of the zero-intensity minimum of the RESOLFT focus can effectively assume the fluorescent (ON) state and hence contribute to the fluorescence signal.

The diameter of this ON-state area is given by

$$d \approx \frac{\lambda}{2n \sin \alpha \sqrt{1 + I/I_s}} \quad (1)$$

with  $\lambda/(2n \sin \alpha) = \Delta$  being the conventional resolution ( $\sim 200\text{--}300\text{nm}$ ), and  $I$  denoting the illumination intensity at the ring crest. Hence, features that are (just slightly) more apart than  $d$  but less than  $\Delta$  cannot fluoresce at the same time although they will be illuminated by the same diffraction-limited pattern of excitation light. The intensity  $I$  must exceed the threshold  $I_s \sim C\tau^{-1}$  with  $C$  accounting for the probability of a RESOLFT beam photon to switch the fluorescent protein into the dark state. Since the switching of rsFPs in RESOLFT involves a long lived dark state with a lifetime  $\tau$  of  $\mu\text{s--ms}$ , the light intensity involved in the imaging process will be in the  $\text{W/cm}^2\text{--kW/cm}^2$  range, which is several orders of magnitude lower than in other nanoscopy approaches, such as STED. Scanning the on- and off-switching beams jointly with a regularly focused excitation beam across the specimen ensures that features that are closer than the diffraction barrier assume the fluorescent state sequentially in time, and are thus separated. RESOLFT is a direct superresolution method because it immediately renders high resolution images without any mathematical reconstruction. Together with the minimal light intensities required in the image recordings, this feature makes RESOLFT highly appealing for many applications in cell and tissue imaging.

## $\tau$ - RESOLFT experimental platform

We modified our home-built RESOLFT microscope<sup>3</sup> for measuring fluorescence lifetimes. The microscope utilized three separate beam paths for generating co-aligned focal spots: two at 491 nm wavelength for excitation and OFF-switching, and one at 405 nm for ON-switching.

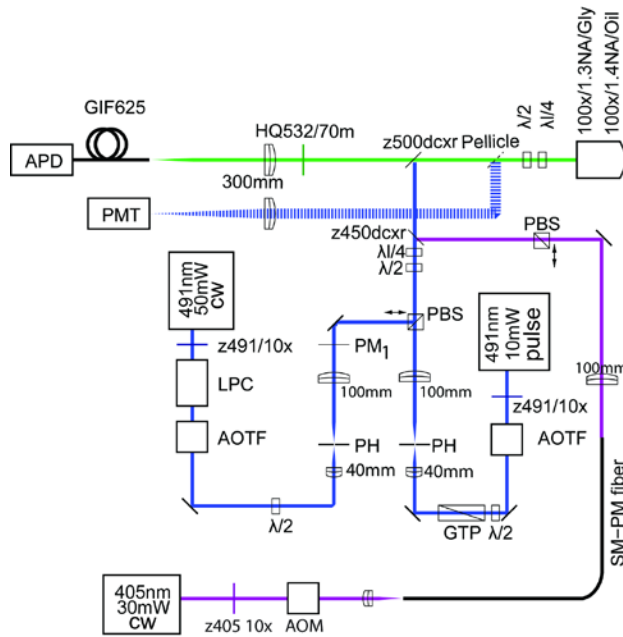


**Figure S1.** Scheme of our  $\tau$ -RESOLFT microscope composed of several lenses, filters and the following optical components: AOM, acousto optic modulator; AOTF, acousto optic tunable filter; LPC, laser power controller; PH, pinhole; PM, phase mask; GTP, Glan-Thompson polarizer;  $\lambda/2$  and  $\lambda/4$  half and quarter wave plates. PMT, photomultiplier tubes; APD, single photon avalanche photodiode. SM-PM, single-mode polarization maintaining fiber, GIF625, multi-mode fiber.

The two focal spots at 491 nm comprised: (i) a normally focused pulsed beam for reading out the fluorescence signal; (ii) a ‘doughnut-shaped’ focal intensity distribution with a central minimum (‘zero’) for OFF-switching at the focal periphery in the xy-plane, obtained by passing a continuous-wave beam through a vortex phase mask (463nm mask, vortex plate VPP-A, RPC Photonics, Rochester, NY). The two focal intensity spots were generated by two different laser diodes (50 mW, continuous wave, Calypso 50, Cobolt, Stockholm, Sweden) for OFF-switching and (10mW, 80–100ps pulse width, PicoQuant, Berlin, Germany) for fluorescence readout. The third focal spot, again with a regularly focused profile, was generated by a laser diode at 405nm wavelength (30mW, BCL-030-405-S, CrystaLaser, Reno, NV, USA) and used for the ON-switching of the fluorescent protein. Two separate objective lenses were used alternatively in this setup: an oil-immersion lens (HCX PC APO, 100 $\times$ , 1.4NA, oil; Leica Microsystems, Wetzlar, Germany) was used only when imaging neuronal features within 5 $\mu$ m of the tissue surface (only for experiments on neuronal cultures), and a glycerol-immersion lens (PL APO, CORR CS, 63 $\times$ , 1.3NA, glycerol; Leica

Microsystems) was used in order to penetrate deep enough into the tissue sample. Using this lens we imaged DronpaM159T and rsEGFPN205S labelled neurons between 30–50  $\mu\text{m}$  deep inside brain slices. The correction collar of the glycerol objective lens was adjusted for each specific imaging depth by maximizing the fluorescence signal and minimizing the effective point spread function along the optical (z-) axis. A piezo actuator (ENV40/20, Piezosystem Jena, Jena, Germany) was used to move the objective lens along the optical axis in a range of 120  $\mu\text{m}$ . A separate piezo stage (NV40, Piezosystem Jena) was implemented to translate the sample with nanometer precision in the xy-plane. The fluorescence signal was filtered by a bandpass filter (532/70 nm) and detected by an epitaxial silicon single photon avalanche diode SPAD (MPD, Bolzano, Italy); fluorescence photons were counted only when the 491nm pulse read-out beam was switched on. The individual laser beam paths were triggered either by an acousto-optic modulator (MTS 130A3, Pegasus Optik GmbH, Wallenhorst, Germany) or by an acousto-optic tunable filter (AOTF.nC/TN, Pegasus Optik GmbH). The pulse sequence and duration were defined by a pulse generator (Model 9514, QUANTUM COMPOSERS, Bozeman, MT, USA) and triggered by a time-correlated single photon counting module (Becker & Hickl, Berlin, Germany) pixel by pixel.

### **Imaging acquisition and lifetime separation.**

Image acquisition was performed with the software ImSpector ([www.imspector.de](http://www.imspector.de)). Each image was recorded by applying a specific pulse scheme, pixel by pixel. The laser intensities used in our illumination scheme ranged between 0.4 and 10  $\text{kW}/\text{cm}^2$ . The pixel dwell-time was adjusted according to the illumination intensities and ranged between 500–1000  $\mu\text{s}$ , including 50 $\mu\text{s}$  irradiation at 405nm (1–2  $\text{kW}/\text{cm}^2$ ), 300–800 $\mu\text{s}$  for switching off at 491nm (0.4–8  $\text{kW}/\text{cm}^2$ ) and 50–100 $\mu\text{s}$  to read out the fluorescence signal (0.4–10  $\text{kW}/\text{cm}^2$ ). The fluorescence lifetime of the reported green-emitting reversible switchable fluorescent proteins is typically in the 0.6–2ns range. When two proteins are selected from the upper and lower end of this range, respectively, the differences are usually sufficient to discriminate them by lifetime (see Figures S3 and S7). The fluorescence decay histogram (256 bins for a 12.5ns time window) was analyzed with a bi-exponential decay function which is a generalization of the model introduced in <sup>4</sup>.

The fluorescence decay was deconvolved with the instrument response function (IRF) which was measured by acquiring a time correlated single photon counting (TCSPC) histogram from light reflected by a mirror. To fit the model function to the measured TCSPC histograms

a custom routine was written in MATLAB (The Mathworks, Natick, MA, USA) which implements a maximum likelihood estimator (MLE) assuming Poissonian statistics<sup>4</sup>. In our dual-channels RESOLFT separation experiments the fluorescence lifetimes of each component was fixed. These lifetime values were measured in previous experiments on samples expressing Dronpa or rsEGFP, fused with the protein of interest.

A double exponential function with fixed lifetime and background values is used to fit the photons of each image pixel. The per-pixel amplitudes reflect the distribution of the two fluorescent proteins.

### $\tau$ -RESOLFT recording data set

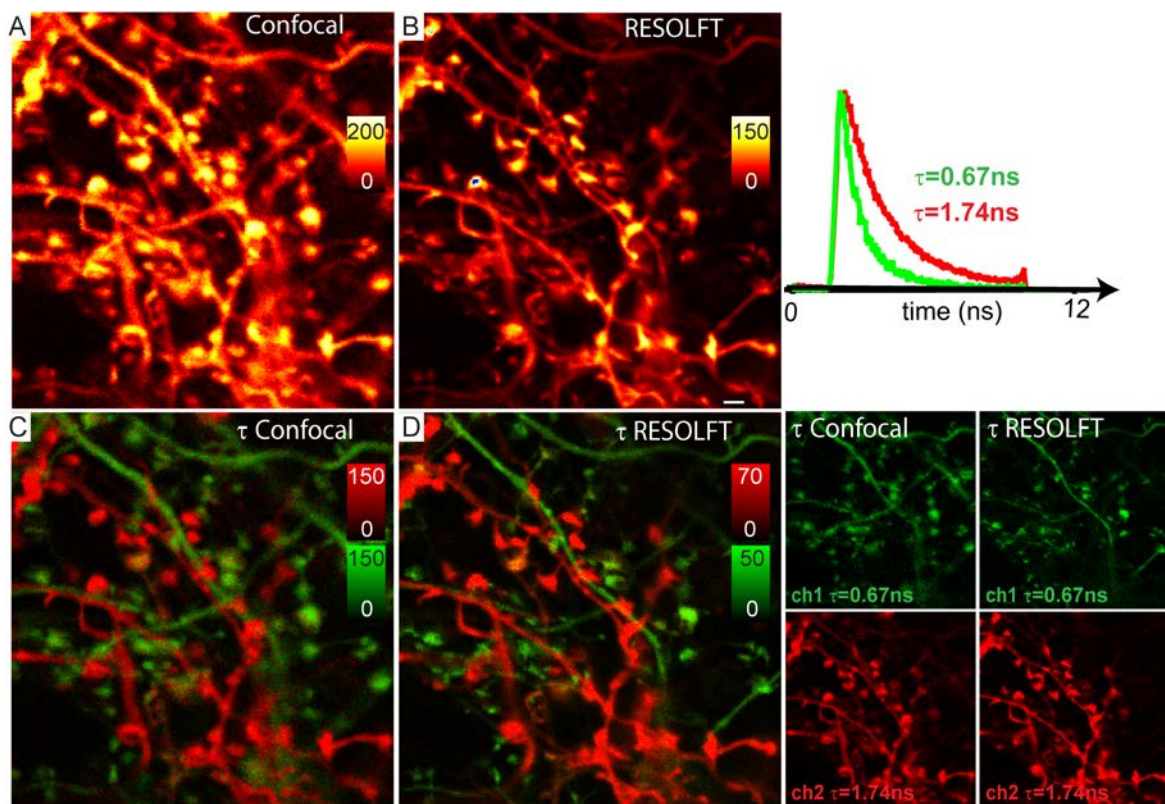


**Figure S2.  $\tau$ -RESOLFT complete data set.** Confocal (A) and RESOLFT (B) images of a brain slice. Each image has in the third dimension the information of the fluorescent photon arrival time (256 bins for 12.5ns time interval). Both images are raw data. The reversible switchable fluorescent proteins Dronpa and rsEGFP, show different fluorescent lifetime values  $\tau=0.67\text{ns}$  and  $\tau=1.74\text{ns}$ . This information is used to separate two species of neuronal proteins, homer1c and LifeAct fused with Dronpa and rsEGFP respectively. The confocal (C) and RESOLFT (D) lifetime separated channels are shown in green for Dronpa and in red for

rsEGFP labelled molecules. Pixel size and dwell time are 100nm and 100 $\mu$ s (A, C) and 30nm and 500 $\mu$ s (B, D). Scale bar 1 $\mu$ m.

### Fluorescence lifetime of green-emitting rsFPs for RESOLFT nanoscopy

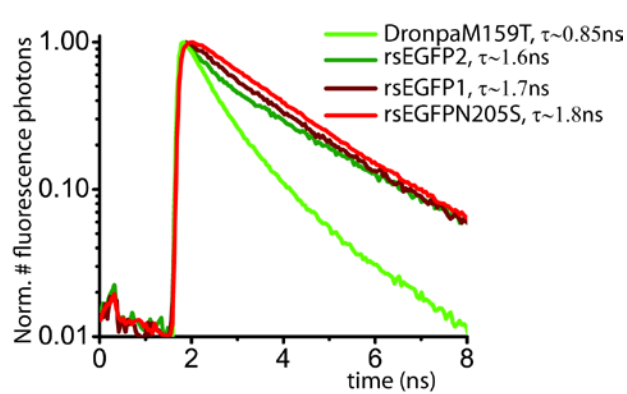


**Figure S3.** Fluorescence lifetime curves of green-emitting reversible switchable fluorescent proteins suitable for RESOLFT nanoscopy. Displayed semilogarithmically, the data was measured directly in living cells expressing keratin labelled with the rsFP indicated. The fluorescence lifetime values, extrapolated from a

monoexponential decay fitting, are in the range of 0.85–1.8ns. We selected DronpaM159T and rsEGFPN205S, because the difference in their fluorescence lifetime was enough to separate them.

### Separation performance for different photon counts

In order to test the performance of the lifetime separation into two species, a simulated lifetime image was constructed by combining photon counts originating from each species (Figure S4, A). A photon count span from 0 to 200 was assigned to each species, with lifetime values of 0.8ns (channel 1, red, horizontally increasing) and 1.6ns (channel 2, green, vertically increasing).

Each pixel of the image was generated by taking a given number of photons for each species and distributing them along the time axis according to their corresponding probability density function. These functions were constructed by convolving the respective mono-exponential decay with the empirical instrument response function in order to reproduce realistic experimental conditions.

We tested the separation ability of the algorithm by generating a stack of 100 lifetime images as described above and separating each one of them into the desired channels. Image B shows the merge of the separated channels (image C), which are shown averaged across the 100 stacks.

Each horizontal line profile  $h$  in image B corresponds to an increasing number of photons in channel 1, while having a constant amount of photons assigned to channel 2. Conversely, each vertical line profile  $v$  corresponds to an increasing number of photons in channel 2 and a constant amount of photons assigned to channel 1.

In graph D we plotted the line profile  $h_1$  (empty red squares) which represents the pixels that have full span of photon counts assigned to channel 1 and fixed zero photons in channel 2. The separated data is in agreement with the original data with a minimal error comparable to the Poissonian noise ( $\pm\sigma$  in dotted lines) present in raw data. This implies that the separation procedure does not add significant noise to the images. Since the effective PSF is the same in raw data as in separated data, we also conclude that the spatial resolution does not deteriorate.

Graph E shows the same type of analysis for the vertical line profile  $v_1$  (empty green square), where channel 2 photon counts increase from 0 to 200 and channel 1 is fixed at 0 photons.

By taking the ratio between the separated channels of these profiles we obtain the crosstalk curves versus the photon counts (Graph F), which are in agreement with the crosstalk fraction measured directly in the real data (Supplementary figure S8). In order to have a general understanding about the separation ability for different photon count pairs in channels 1 and 2, we plotted additional horizontal and vertical profiles. Graphs G and H show the separated photon counts for channel 1 along the horizontal line profiles  $h_1, h_2, h_3$  (Graph G) and all the vertical profiles (Graph H). As the counts in channel 2 increase, a positive offset (below the 10%) in the separated photon counts with respect to the assigned counts is produced. Graphs I and L show the separated photon counts for channel 2 along the vertical line profiles  $v_1, v_2, v_3$  (Graph I) and all the horizontal profiles (Graph L). Again, an offset in the number of separated counts is observed, but in this case is negative and mostly a constant 10%.

Though this systematic biasing of the count estimation could be corrected, it has been neglected as it is found to be of the order of the Poissonian noise. In the graphs of M we plot the histogram of separated counts for each channel, where the total number of photons is always 50. Each histogram corresponds to a different pair of photons values on each channel: (50, 0), (40, 10), (30, 20), etc. Interestingly the shape of the distributions changes for different pair values, going from peak-like to bell-shaped as the values of photons become similar. The open circles indicate the mean of the distributions with the crossing line representing the uncertainty ( $\pm\sigma$ ). The filled circles and the black bar are the median and the expected value, respectively.

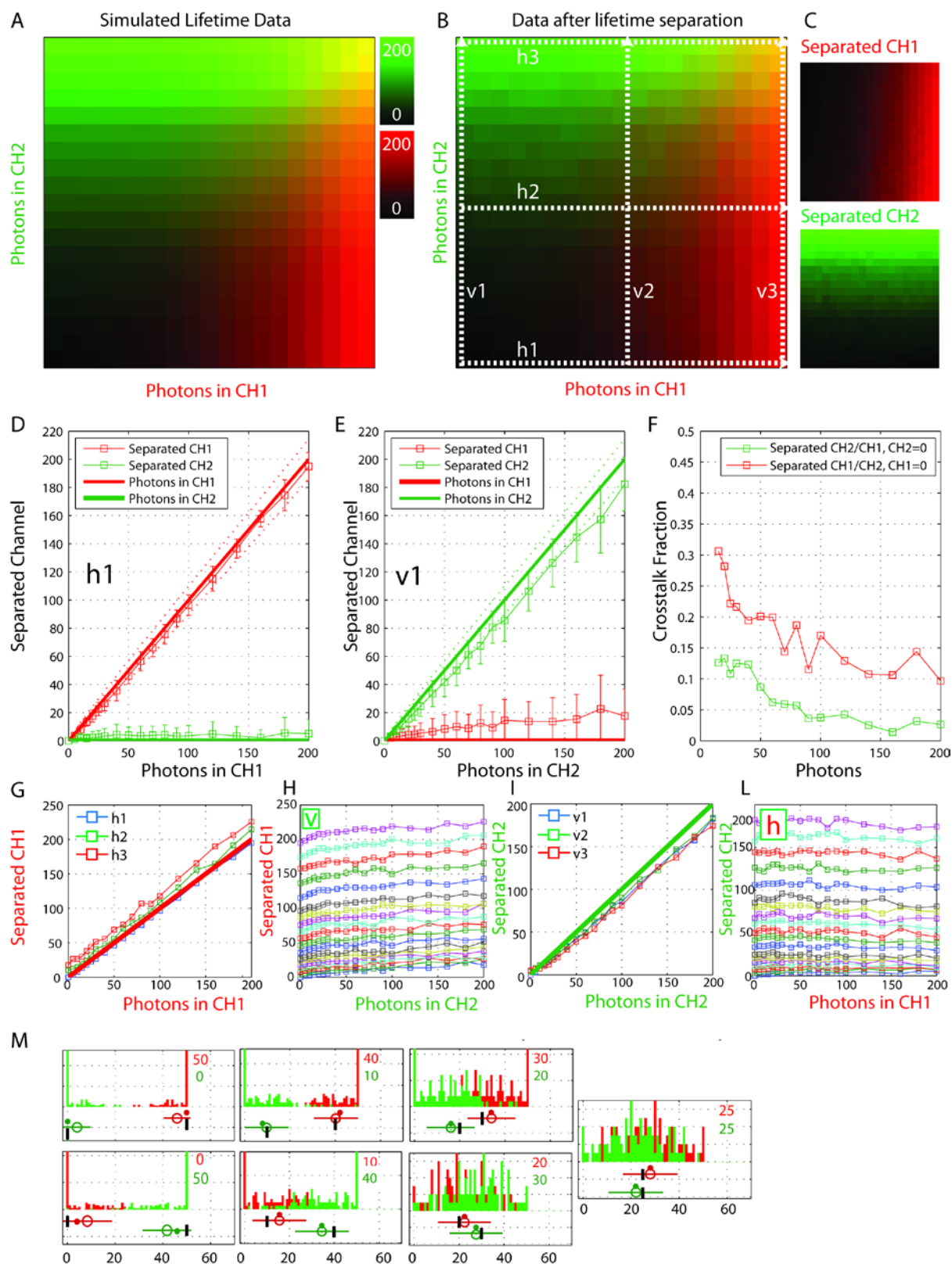


**Figure S4.** Simulated image having  $20 \times 20 \times 100$  pixels with different photon counts (0–200) for lifetimes  $\tau_1 = 0.8\text{ns}$  (red) and  $\tau_2 = 1.6\text{ns}$  (green) (A). This image was analyzed by our lifetime algorithm and separated in two channels, 1 and 2, depending on the pixel counts (B, C).

Graph D shows the horizontal line profile along h1 (with 0 photons in channel 2) while Graph E shows the vertical line profile along v1 (with 0 photons in channel 1). Graph F shows the crosstalk fraction of both channels depending on the photon counts.

Graphs G and H show the photons (0–200) assigned to channel 1 for different amounts of photons in channel 2. Conversely, graphs I and L show the photons (0–200) assigned to channel 2 for different amounts of photons in channel 1.

The histograms plotted in M in red and green show how multiple pixels with the same given photon counts for  $\tau_1$  and  $\tau_2$  (for example (0,50)) are separated by the algorithm. The mean, standard deviation and median of 7 representative distributions are plotted (open circles, crossing lines, filled circles) compared to the expected value (black bars) shown at the bottom of the graph for the green and red distributions.

### rsEGFP and Dronpa switching to the off state

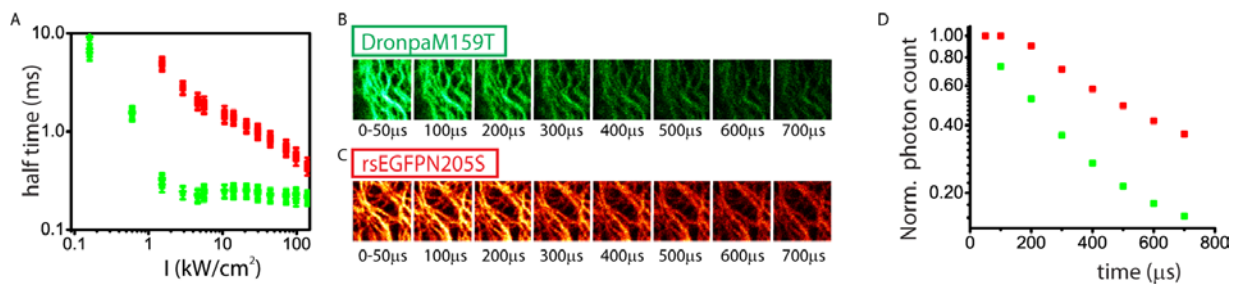


**Figure S5.** Although spectrally nearly identical, DronpaM159T and rsEGFPN205S differ in kinetics when switching to their dark state. The Dronpa population (green square dots in graph A, semilogarithmic scale) switches 16 times faster at low intensity and 2 times faster at higher intensities than the rsEGFPN205S (red square dots in graph A).

Each point of graph A is the half time of an exponential decay function used to fit the switching-off decay curves measured at different blue laser intensities.

This difference can be used to further separate their fluorescence signal during the imaging process. In fact, a gated fluorescence detection in the  $\mu\text{s}$  time window (B, C) showed a faster decay of the signal generated by Dronpa (green squares, graph D) compared to rsEGFP (red square, graph D). Note that this gating is carried out on the switching time scale (50–100  $\mu\text{s}$ ) which is 5–6 orders of magnitude longer than that of the fluorescence lifetime (0.85–1.8 ns).

The experiments were performed in living cells expressing the rsFPs fused with keratine.

A second aspect of the switching kinetics under blue light exposure is the amount of fluorescent photon detectable before the proteins switch to the off state.

These values are determined by calculating the integral of the switching-off curves. We considered the brightness of the Dronpa and rsEGFP variants to be comparable, so we measured the fluorescent photons emitted by both proteins populations by averaging 100 switching cycles.

The rsEGFP population emits 24 times more photons compared to the Dronpa population, when exposed to blue light of intensity equal to  $3.3\text{kW/cm}^2$  for 8ms. However, in a typical read-out time of  $100\mu\text{s}$  this difference scales down to a factor of 1.5 times more fluorescent photons detected from the rsEGFP compared to the Dronpa population. This minor difference can be exploited to image proteins expressed in the cell environment with different abundance. For example, the less abundant protein can be fused with rsEGFP to achieve a fluorescent signal comparable to the Dronpa fusion protein.

### Time and spatial resolution for rsEGFP and Dronpa RESOLFT imaging

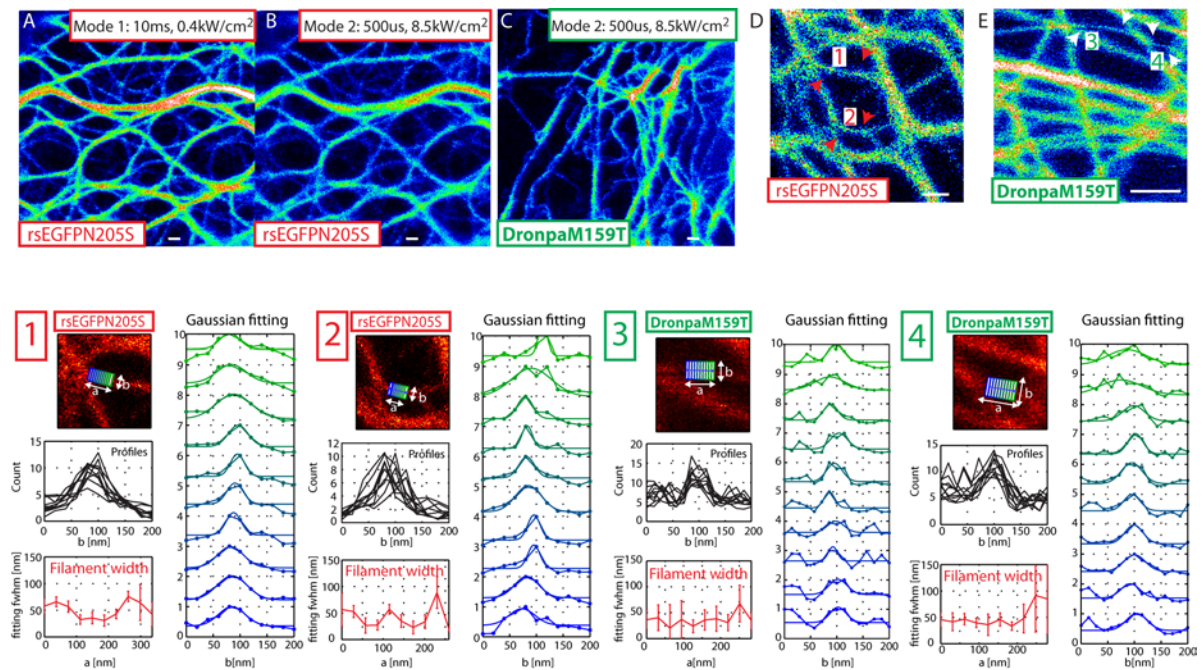


**Figure S6.** Cells expressing rsEGFP and Dronpa fused with keratin were imaged with different parameters. The RESOLFT images A and B, recorded with different switching-off laser duration and intensities as indicated, show comparable spatial resolution. However, the rsEGFPN205S population can perform a larger number of cycles ( $>2000$ ) at lower intensities (Mode 1,  $\sim 0.4\text{kW/cm}^2$ ) yielding a better signal-to-noise ratio. Therefore, the configuration of image A (Mode 1), i.e. low switching intensity and longer switching-off time, can image dimmer structures at the expense of time resolution. In our experiment we selected the

configuration of images B and C (Mode 2) as a good compromise between spatial and temporal resolution.

The spatial resolution was measured in two keratin filaments fused with rsEGFP (D, 1 and 2) and in Map2 filaments fused with Dronpa (E, 3 and 4). Pixel size of images D and E are 20nm and 15nm respectively. Scale bar 500nm.

Four filaments were analyzed with 10 perpendicular line profiles (400nm long), each one averaging 3 neighboring pixels in order to reduce noise artifacts.

Each profile was fitted with a Gaussian curve and the resulting FWHM is reported with the fitting errors in the relative “filament width” graphs (red curves).

The faster switching protein, in this case DronpaM159T, will always be slightly better resolved than its slower counterpart (rsEGFPN205S), as the lower switching threshold of the faster protein results in a smaller focal region in which the protein is in the ON-state. This imperfection decreases with decreasing size of this region, i.e. with increasing resolution. It basically disappears at resolutions  $< 50$  nm, as observed here. It can be eliminated by using an rsFP pair with similar switching kinetics to the ON and OFF states ( $\mu\text{s}$ – $\text{ms}$  range) and different fluorescence lifetime (ns range).

### Fluorescence lifetime distributions in living neurons

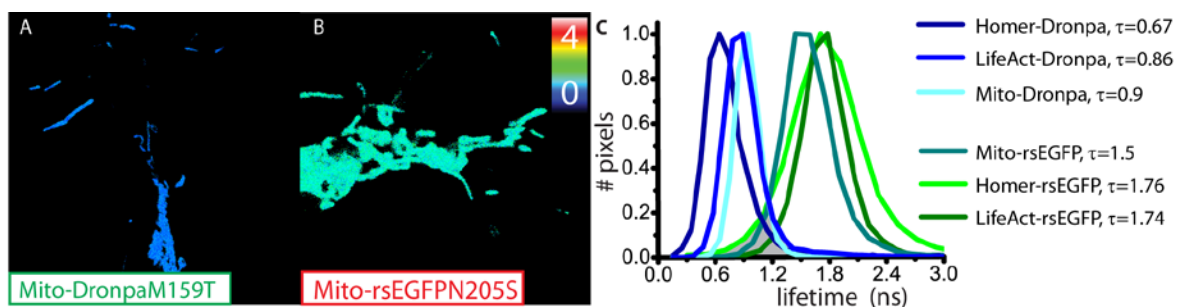


**Figure S7.** Fluorescence lifetime distributions of Dronpa and rsEGFP in living cells. Images A and B show the lifetime distributions of the Dronpa and rsEGFP variants in mitochondria, respectively. The fluorescence lifetime values (0–4 ns) of each pixel, extrapolated from a monoexponential fit, lead to the normalized distributions plotted in graph C. The center of the distribution is  $\tau=0.9\text{ns}$  for mito-DronpaM159T and  $\tau=1.5\text{ns}$  for mito-rsEGFPN205S. The overlapping area of the two distributions, 10% and 15% of their total area, is an indicator for the error in the channel assignment. The center and the size (FWHM 0.5) of the distribution can vary in different cellular environments. For example, the lifetime distributions of homer-

DronpaM159T and LifeAct-rsEGFPN205S labelled structures show shifted lifetime values  $\tau=0.67$  and  $\tau=1.74$ , which are separated with a minimal error  $<3\%$ .

### Crosstalk evaluation

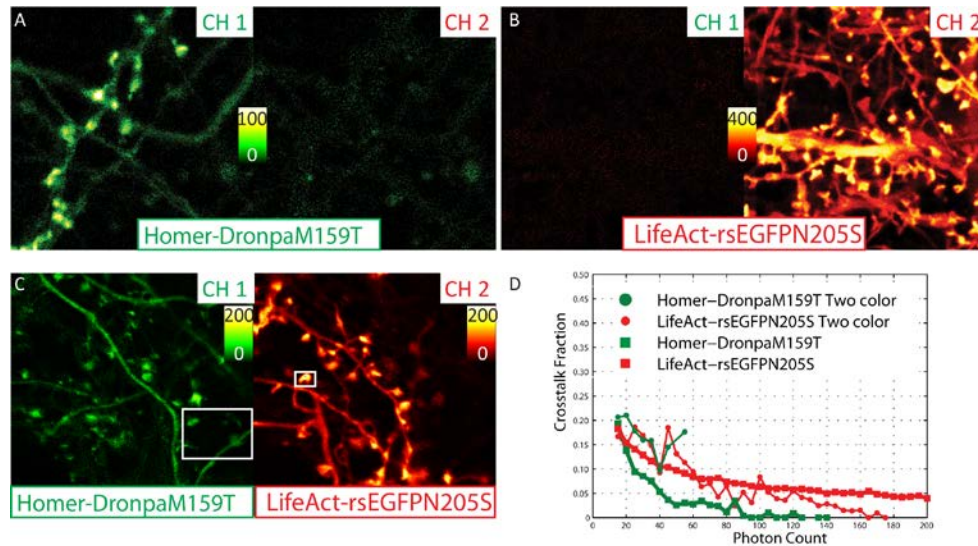


**Figure S8.** Signal separation by fluorescence lifetime of Dronpa (ch1) and rsEGFP (ch2). Image A shows the signal of both

channels for neurons transfected only with homer1c-DronpaM159T. Channel 2 displays wrongly assigned photons accounting for the crosstalk. The average crosstalk ( $ch2/ch1+ch2$ ) for sets of pixels with comparable photon count is shown in graph D (green squares). The crosstalk depends on the total photon counts: pixels with low counts ( $<20$  photons) show higher crosstalk values ( $\sim 20\%$ ) than brighter pixels ( $<1\%$ ). Neurons uniquely transfected with LifeAct-rsEGFPN205S were imaged and separated in image B. The crosstalk for ch1 ( $ch1/ch1+ch2$ ) is plotted in graph D (red squares). Neurons transfected with both constructs (homer1c-DronpaM159T and LifeAct-rsEGFPN205S) are shown in image C. Their crosstalk behavior, measured in the regions highlighted in the white boxes, is plotted in green and red circles for ch1 and ch2, respectively.

1. Gahwiler, B. H.; Capogna, M.; Debanne, D.; McKinney, R. A.; Thompson, S. M. *Trends Neurosci* **1997**, 20, 471-477.
2. Urban, N. T.; Willig, K. I.; Hell, S. W.; Nagerl, U. V. *Biophys J* **2011**, 101, 1277-84.
3. Testa, I.; Urban, N. T.; Jakobs, S.; Eggeling, C.; Willig, K. I.; Hell, S. W. *Neuron* **2012**, 75, 992 - 1000.
4. Maus, M.; Cotlet, M.; Hofkens, J.; Gensch, T.; De Schryver, F. C.; Schaffer, J.; Seidel, C. A. M. *Anal Chem* **2001**, 73, 2078–2086.